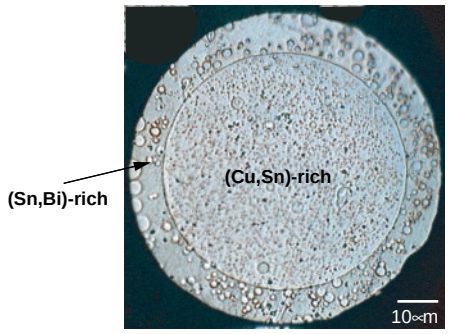


**Fig. 4.** Microstructure of the 24Cu-16Sn-60Bi (weight %) alloy powder.

shown in Fig. 4, indicating the egg-type structure of Cu-Sn–rich core with a Sn-Bi–rich periphery. The commercial size of a Cu core ball plated with Pb-Sn eutectic solder is ~700 μm, but a size of <100 μm is required for the chip-scale package, which is very difficult to produce by the conventional plating method. As shown in Fig. 4, the size of egg-type powder is ~80 μm.

The egg-type powder can be obtained in many alloy systems that possess a liquid miscibility gap. This simplified fabrication method may open up new applications for these alloy materials.

### References and Notes

1. B. Predel, in *Thermodynamics of Alloy Formation*, Y. A. Chang and F. Sommer, Eds. (Minerals, Metals and Materials Society, Warrendale, PA, 1997), pp. 1–19.
2. L. Ratke, S. Diefenbach, *Mater. Sci. Eng.* **R15**, 263 (1995).
3. H. Ahlborn, K. Löhberg, in *17th Aerospace Sciences Meeting* (American Institute of Aeronautics and Astronautics, New York, 1979), pp. 3–7, paper 79-0172.
4. B. Predel, L. Ratke, H. Fredriksson, in *Fluid Sciences and Materials Science in Space*: *A European Perspective*, H. U. Walter, Ed. (Springer-Verlag, New York, 1987), pp. 517–565.
5. B. Prinz, A. Romero, L. Ratke, *J. Mater. Sci.* **30**, 4715 (1995).
6. C. P. Wang, X. J. Liu, I. Ohnuma, R. Kainuma, K. Ishida, *J. Phase Equilibria* **23**, 236 (2002).
7. N. O. Young, J. S. Goldstein, M. J. Block, *J. Fluid Mech.* **6**, 350 (1959).
8. L. Ratke, P. W. Voorhees, in *Growth and Coarsening* (Springer-Verlag, New York, 2002), pp. 239–249.
9. C. Marangoni, *Ann. Phys. Chem.* **143**, 337 (1871).
10. R. Becker, *Ann. Phys.* **32**, 128 (1938).
11. T. Nishizawa, I. Ohnuma, K. Ishida, *J. Phase Equilibria* **22**, 269 (2001).
12. Q. Chen, Z. P. Jin, *Metall. Mater. Trans. A* **26A**, 417 (1995).
13. S. Seetharaman, D. Sichen, *Metall. Mater. Trans. B* **25B**, 589 (1994).
14. S. J. Jamil, G. A. Chadwick, *Powder Metall.* **28**, 65 (1985).
15. E. Bradley, K. Banerji, *IEEE Trans. Components Packag. Manuf. Technol.* **B19**, 320 (1996).
16. S. Kiyono, K. Uenishi, K. Kobayashi, I. Shohji, M. Yamamoto, *J. Jpn. Inst. Electron. Packag.* **2**, 298 (1999).
17. I. Ohnuma, X. J. Liu, H. Ohtani, K. Ishida, *J. Electron. Mater.* **28**, 1163 (1999).
18. We thank Daido Steel Company for preparing the powders. Partially supported by a Grant-in-Aid for the Development of Innovative Technology.

18 April 2002; accepted 3 July 2002



# Dipole Moments of Highly Vibrationally Excited Water

**Andrea Callegari,[1] Patrice Theulé,[1] John S. Muenter,[2] Roman N. Tolchenov,[3] Nikalai F. Zobov,[3]* Oleg L. Polyansky,[3]* Jonathan Tennyson,[3] Thomas R. Rizzo[4]†**

**The intensity of water absorption in the region of the solar spectrum plays a dominant role in atmospheric energy balance and hence strongly influences climate. Significant controversy exists over how to model this absorption accurately. We report dipole moment measurements of highly vibrationally excited water, which provide stringent tests of intensities determined by other means. Our measurements and accompanying calculations suggest that the best currently available potential and dipole surfaces do not accurately model intensities in the optical spectrum of water.**

The absorption of solar energy by molecules in the Earth's atmosphere and the subsequent energy transfer processes are of enormous importance in understanding global climatology. Despite the immense amount of experimental and theoretical work incorporated into atmospheric models, as much as 30% of solar radiant flux is not accounted for (*1–4*). Water is the dominant absorber in the Earth's atmosphere and plays a central role in climate evolution. However, this role is complicated and difficult to quantify, and there is substantial controversy over how well water absorption is modeled (*5–8*). Much of the controversy arises from the near-infrared (near-IR), visible, and near-ultraviolet (near-UV) portions of the spectrum, where water exhibits large numbers of weak spectroscopic transitions. These features occur at the peak of the solar spectrum and contribute a significant fraction of the total solar energy deposited in the atmosphere (*9*). Because the small intensities of the individual absorptions are difficult to measure accurately, theoretical calculations of water absorption profiles in these spectral regions can improve atmospheric models. However, the accuracy of these calculations must be independently confirmed for this approach to gain widespread acceptance. A number of other fields would also benefit from a better understanding of the water absorption spectrum, including the study of sunspots (*10*), cool star evolution (*11*), and rocket exhausts (*12*), as well as other disciplines in which water occurs in extreme environments.

The absorption spectrum of water, from the far-IR to the near-UV, is controlled by its electric dipole moment and the changes of this moment with vibrational motions. Molecular vibrations are specified by the potential energy surface (PES), which provides the total energy as an analytic function of internal coordinates used to describe molecular geometries. Similarly, the first moment of the charge distribution is given by the dipole moment surface (DMS). High-quality potential and dipole surfaces are both needed for the calculation of spectral intensities. Techniques for combining ab initio computations and experimental spectra to produce potential energy surfaces are well developed, and accurate potentials exist for water (*13, 14*), including those that go beyond the Born-Oppenheimer approximation (*15*).

The situation is less advanced for dipole moment surfaces. Ab initio calculations of dipole moments converge differently from those of energies and hence do not obey the variational principle. Thus, calculations that give comparable energies can produce quite different moments (*16–18*). Even when high-quality dipole moment calculations exist for a broad range of configurations, the choice of how to best parameterize the DMS is not trivial (*19*). Empirical DMSs rely on absolute spectroscopic intensity measurements, which are notoriously difficult to carry out with high accuracy. Moreover, it is surprisingly difficult to prepare simulated atmospheric samples containing accurately known densities of water (*20*). Even if one could measure accurate intensities, it is difficult to determine an accurate DMS from intensity measurements alone, as the inversion process would require an extremely accurate PES (*21*). Better modeling of the water absorption spectra, particularly the weak transitions in the visible and UV regions, requires new sources of accurate dipole moment data that can test and refine both ab initio and empirical DMSs. Perma-

[1]Laboratoire de chimie physique moléculaire (LCPM), École Polytechnique Fédérale de Lausanne, 1015 Lausanne, Switzerland. [2]Department of Chemistry, University of Rochester, Rochester, NY 14627, USA. [3]Department of Physics and Astronomy, University College London, Gower Street, London WC1E 6BT, UK. [4]Laboratoire de chimie physique moléculaire (LCPM), École Polytechnique Fédérale de Lausanne, 1015 Lausanne, Switzerland.

*Permanent address: Institute of Applied Physics, Russian Academy of Sciences, Uljanov Street 46, Nizhinii Novgorod, Russia 603950.
†To whom correspondence should be addressed. E-mail: thomas.rizzo@epfl.ch

nent dipole moments obtained from spectroscopic measurements of the Stark effect (*22*) can be highly accurate and do not depend on sample conditions (*23–25*). Stark coefficients can have accuracies better than 0.1%, in contrast to long path absorption measurements where 10% uncertainties are typical. Stark measurements of ground state and low-lying excited-state moments have been used to improve the water DMS for geometries near equilibrium (*26*). However, the regions of the DMS most relevant to the visible and UV water spectrum involve geometries far from equilibrium, in particular near the inner wall of the potential (*27*). Dipole moment data from high vibrational states provide a probe sensitive to large portions of configuration space and serve to improve the DMS globally, including those geometries relevant to the absorption spectrum.

We present measurements of Stark coefficients and electric dipole moments of highly excited vibrational states of water. These experiments combine the technique of vibrationally mediated photodissociation (*28, 29*) with pump and probe quantum beat spectroscopy (*30*), to make Doppler-free measurements of Stark-induced splittings within highly excited quantum states. The results of these experiments are used to test some of the best PESs and DMSs currently available.

All of the experiments presented here were carried out on water molecules in rotational states having one unit of angular momentum ($J = 1$). When placed in a laboratory electric field, $E$, $J = 1$ energy levels split into two components, $J = 1$, $M = 0$ and $J = 1$, $M = \pm 1$, which have different energies and spatial orientations. The energy difference between the $M = 0$ and $M = \pm 1$ components, $\Delta W = W_0 - W_1$, is called the Stark splitting and is commonly written in frequency units as $\nu = \Delta W/h$. The Stark splitting is proportional to $E^2$ (*22*), so we write $\nu = CE^2$ and refer to $C$ as the Stark coefficient of the state being studied. Because $C$ is directly related to the permanent dipole moment of the molecule (*22*), experimentally observed Stark coefficients are the standard source of dipole moment data.

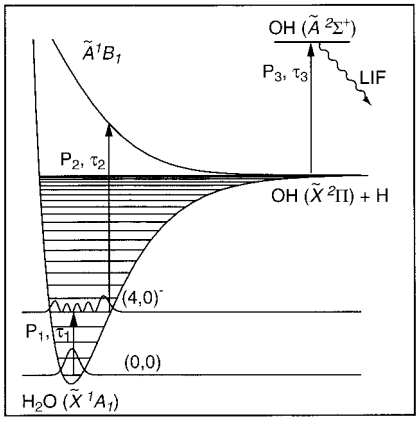


**Fig. 1.** Schematic energy level diagram describing the excitation scheme used to observe quantum beats in the $(4,0)^-$, $1_{10}$ state of water. Wavelengths and typical delay times are: $\lambda_1 =$ 725 nm, $\lambda_2 =$ 266 nm, $\lambda_3 =$ 308 nm, $\tau_2 - \tau_1 =$ 400 ns, and $\tau_3 - \tau_2 =$ 20 ns.

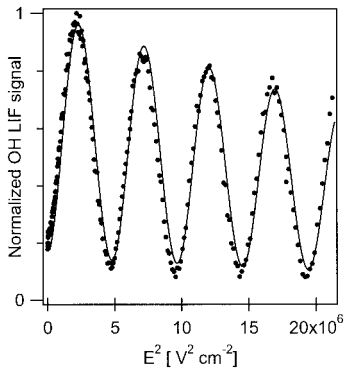


**Fig. 2.** Stark-induced quantum beats in the $(4,0)^-$, $1_{10}$ state of water for $\Delta t = 405.6$ ns. Data are shown as filled circles. The solid line is $S = (k_1 - k_2E)[1 - k_3\sin(2\pi CE^2\Delta t + \phi)]$, where $k_1$ through $k_3$ are parameters describing the slope and decay of the quantum beats, $\phi$ is a phase angle, and $C$ is the desired Stark coefficient.

We measure the Stark splitting, $\nu$, using Nd:yttrium-aluminum-garnet lasers with pulse widths of about 10 ns. In the example shown in Fig. 1, the experiment begins with a pulse $P_1$, at time $\tau_1$, which excites a $J = 1$ level of a vibrational state having four quanta of O-H stretch. In the presence of an external electric field, the 10-ns laser pulse creates a wave packet containing both $J = 1$, $M = 0$ and $J = 1$, $M = \pm 1$ states. Classically, this wave packet precesses around the direction of the dc electric field at a frequency equal to the Stark splitting, $\nu$ (*31*). The alignment of the wave packet at a later time $\tau_2$ is detected with a second laser pulse, $P_2$, which excites water molecules to the repulsive $A^1B_1$ electronic state, where they immediately dissociate to form OH + H photofragments (*28, 29*). The efficiency of this laser-induced photofragmentation depends on the alignment of the wave packet relative to the polarization of $P_2$ (*32*). The concentration of OH radicals generated by $P_2$ depends on how far the wave packet has precessed in the time interval $\Delta t = \tau_2 - \tau_1$. The OH radicals created by $P_2$ are detected with a third laser pulse, $P_3$, occurring at time $\tau_3$, which generates an OH laser-induced fluorescence (LIF) signal (*28, 29*).

We monitored the OH LIF signal as we scanned the strength of the applied field, $E$, at a fixed value of $\Delta t$ (*33*). The polarization of the laser pulse $P_2$ was chosen to produce a minimum OH signal when $E = 0$, corresponding to a zero precession frequency. The electric field value that generates one-half revolution of precession in the time period $\Delta t$ produced a maximum LIF signal. Increasing E to double the precessional frequency, $\nu$, produced a full cycle of rotation in the time $\Delta t$, which again gave a minimum OH signal. This process was continued for many cycles. Because $\nu = CE^2$, a plot of the LIF signal versus $E^2$ displays the oscillations (i.e., quantum beats) arising from the precessing wave packet (Fig. 2). From these data we extracted accurate Stark coefficients for highly excited states of water.

The vibrational states of $H_2O$ studied here contained 4, 5, or 8 quanta of OH stretch, and are best described with local mode basis functions, (v,0) and (0,v), having all of the excitation in either one or the other of the two identical OH bonds (*34*). For a molecule containing v quanta OH stretch, the observed eigenstates, labeled $(v,0)^+$ and $(v,0)^-$, are respectively the symmetric and antisymmetric linear combinations of the two basis functions (*34, 35*). Using

**Table 1.** Observed and calculated Stark coefficients for water in units of Hz( V/cm)$^{-2}$. The numbers in parentheses are one standard deviation in experimental precision. Absolute accuracy is estimated to be 0.5%. $K_a$ is the approximate projection of the total angular momentum $J$ along the rotational axis with the smallest moment of inertia; $K_c$ is the approximate projection of $J$ along the rotational axis with the largest moment of inertia. $J_{K_aK_c}$ is the quantum number assignment of the vibrational state.

| V | $J_{K_aK_c}$ | $C_{obs}$ | $C_{calc}$ | Percent difference (calc – obs)/obs |
|---|---|---|---|---|
| $(4,0)^-$ | $1_{01}$ | 0.4372(8) | 0.4413 | 0.95% |
| $(4,0)^-$ | $1_{11}$ | 0.3160(9) | 0.2871 | –9.2% |
| $(4,0)^-$ | $1_{10}$ | 0.5097(10) | 0.5060 | 0.72% |
| $(5,0)^-$ | $1_{01}$ | 0.4277(7) | 0.4343 | 1.5% |
| $(5,0)^-$ | $1_{11}$ | 0.3032(7) | 0.2849 | –6.1% |
| $(5,0)^-$ | $1_{10}$ | 0.5077(4) | 0.4996 | –1.6% |
| $(8,0)^+$ | $1_{01}$ | 0.4953(16) | 0.5058 | 2.1% |
| $(8,0)^+$ | $1_{11}$ | 0.4250(10) | 0.4154 | –2.3% |
| $(8,0)^+$ | $1_{10}$ | 0.6.657(38) | 0.6667 | 0.2% |

**Table 2.** Vibrational state dipole moments of water, in Debye.

| | (4,0) | (5,0) | (8,0) |
|---|---|---|---|
| $\mu_b$ | 1.874 | 1.857 | 1.796 |
| $\mu_a$ | 0.291 | 0.344 | 0.584 |

this notation, we report here Stark-induced photofragment quantum beat measurements in the $(4,0)^-$, $(5,0)^-$, and $(8,0)^+$ vibrational states (*36*), using the $1_{01}$, $1_{11}$, and $1_{10}$ asymmetric top rotational levels (*22*) in each case. The nine Stark coefficients observed for the three $J = 1$ levels in three vibrational states are listed in column three of Table 1.

To extract dipole moments from these coefficients, we must consider two particularities related to the near degeneracy of the $(v,0)^-$ and $(v,0)^+$ states that are not included in a conventional Stark analysis. First, an electric dipole transition moment lying along the *a* inertial axis connects these two vibrational states, and this Stark interaction must be included in the analysis. Thus, each observed Stark coefficient depends on both the permanent moment, $\mu_b$, within the vibrational state and the transition moment, $\mu_a$, connecting the $(v,0)^-$ and $(v,0)^+$ vibrational states. The second factor arises because the splitting between $(v,0)^-$ and $(v,0)^+$ is small relative to rotational spacings. This condition requires the use of a Hamiltonian that explicitly contains the local-mode vibrational wave functions. Lehmann (*37*) has developed a Hamiltonian that begins with the two local-mode states, (v,0) and (0,v), and treats simultaneously the interaction between these states and overall molecular rotation. Using this formalism, we obtain the *a* and *b* dipole moment components, listed in Table 2, of the local-mode basis states.

Together with previous measurements for lower vibrational states (*23–25*), our measured permanent and transition dipole moments for $v = 4$, 5, and 8 provide a rigorous test of calculated PESs and DMSs, particularly because the $(8,0)^+$ level is more than halfway to dissociation of the OH bond and has classical turning points extending from –0.25 to +0.6 Å. The most direct way to make this test is to calculate the Stark coefficients and to compare them with the measured values given in Table 1. We chose a PES and DMS and used the variational program DVR3D (*38*) to calculate dipole moment matrix elements. The resulting matrix elements were then squared, combined with experimentally known energy spacings (*39*), and summed to generate the Stark coefficient, *C*. We performed these calculations with various combinations of Partridge and Schwenke's PES (*15*), a newly fitted PES (*40*), the DMS of Partridge and Schwenke (*14*), and the revised DMS of Schwenke and Partridge (*19*). Each combination gave surprisingly similar results, with different *C* values agreeing to within 1%. We consider the *C* values obtained from the most recent PES (*40*) and the revised DMS (*19*) (column four of Table 1) to be the most accurate.

The calculated Stark coefficients differ from our measured values by up to –9.2% [for the $1_{11}$ rotational level of the $(4,0)^-$ state], with those that are most sensitive to $\mu_a$ being consistently too small. These discrepancies do not arise from coincidental connections to other close-lying vibrational states because the nuclear motion calculations explicitly include these interactions (*41*). The percentage differences listed in column five of Table 1 focus attention on limitations of the surfaces used. Four different calculations using two different PESs and two different DMSs gave similar results. The two PESs used (*15, 40*) are completely independent of one another, whereas the two DMSs are different analytical fits of the same set of dipole moment calculations (*14, 19*). This result suggests that the source of discrepancy with experiment is related to the DMS. New ab initio calculations (*42*). with large augmented basis sets (aug-cc-pV6Z) suggest that the Partridge and Schwenke dipole surfaces (*14, 19*) systematically underestimate the water dipole moment as one bond is extended. These are precisely the geometries probed in the current experiments.

Our data, together with the permanent and transition moments derived from them, serve as benchmarks for testing both DMSs and PESs. The best surfaces currently available do not accurately reproduce our results. New DMSs (*42*) and PESs (*40, 42*) that can produce more accurate Stark coefficients should provide a better description of the water absorption spectrum, which is critical for understanding water's role in the Earth's atmosphere.

### References and Notes


1. A. Arking, *Geophys. Res. Lett.* **26**, 2729 (1999).
2. Z. Q. Li, L. Moreau, A. Arking, *Bull. Am. Meteorol. Soc.* **78**, 53 (1997).
3. A. Arking, *Science* **273**, 779 (1996).
4. R. D. Cess *et al.*, *Science* **267**, 496 (1995).
5. E. J. Mlawer *et al.*, *Geophys. Res. Lett.* **27**, 2653 (2000).
6. D. Lubin *et al.*, *J. Geophys. Res. Atmos.* **105**, 22445 (2000).
7. W. Y. Zhong, J. D. Haigh, D. Belmiloud, R. Schermaul, J. Tennyson, *Q. J. R. Meteorol. Soc.* **127**, 1615 (2001).
8. D. Belmiloud *et al.*, *Geophys. Res. Lett.* **27**, 3703 (2000).
9. M. D. Chou, *Terr. Atmos. Ocean. Sci.* **10**, 511 (1999).
10. O. L. Polyansky *et al.*, *Science* **277**, 346 (1997).
11. F. Allard, P. H. Hauschildt, D. R. Alexander, S. Starrfield, *Annu. Rev. Astron. Astrophys.* **35**, 137 (1997).
12. "Terminology and assessment methods of solid propellant rocket exhaust signatures" (NATO Advisory Group for Aerospace Research and Development, Neuilly-sur-Seine, France, 1993).
13. O. L. Polyansky, P. Jensen, J. Tennyson, *J. Chem. Phys.* **105**, 6490 (1996).
14. H. Partridge, D. W. Schwenke, *J. Chem. Phys.* **106**, 4618 (1997).
15. D. W. Schwenke, *J. Phys. Chem. A* **105**, 2352 (2001).
16. A. Halkier, W. Klopper, T. Helgaker, P. Jorgensen, *J. Chem. Phys.* **111**, 4424 (1999).
17. G. de Oliveire, C. E. Dykstra, *Theor. Chem. Acc.* **11**, 435 (1999).
18. H. G. Kjaergaard, K. J. Bezar, K. A. Brooking, *Mol. Phys.* **96**, 1125 (1999).
19. D. W. Schwenke, H. Partridge, *J. Chem. Phys.* **113**, 6592 (2000).
20. R. Schermaul *et al.*, *J. Mol. Spectrosc.* **208**, 43 (2001).
21. A. M. Smith, W. Klemperer, K. K. Lehmann, *J. Chem. Phys.* **94**, 5040 (1991).
22. C. H. Townes, A. L. Schawlow, *Microwave Spectroscopy* (McGraw-Hill, New York, 1955).
23. T. R. Dyke, J. S. Muenter, *J. Chem. Phys.* **59**, 3125 (1973).
24. S. L. Shostak, W. L. Ebenstein, J. S. Muenter, *J. Chem. Phys.* **94**, 5875 (1991).
25. S. L. Shostak, J. S. Muenter, *J. Chem. Phys.* **94**, 5883 (1991).
26. M. Mengel, P. Jensen, *J. Mol. Spectrosc.* **169**, 73 (1995).
27. K. K. Lehmann, A. M. Smith, *J. Chem. Phys.* **93**, 6140 (1990).
28. R. L. Vanderwal, J. L. Scott, F. F. Crim, *J. Chem. Phys.* **94**, 1859 (1991).
29. R. J. Barnes, A. F. Gross, A. Sinha, *J. Chem. Phys.* **106**, 1284 (1997).
30. Related experiments have been performed with different molecules in low-energy vibrational states using fluorescence detection. See H. Bitto, J. R. Huber, *Opt. Commun.* **80**, 184 (1990).
31. In a quantum mechanical picture, this precessing wave packet is more formally described as a coherent quantum beat of frequency, $\nu$.
32. R. N. Zare, *Angular Momentum* (Wiley, New York, 1988).
33. We calibrate the electric field by measuring the distance between the Stark plates using a precision quartz spacer and the applied voltage using a 6-digit HP3456A precision voltmeter together with a calibrated voltage divider.
34. M. S. Child, R. T. Lawton, *Chem. Phys. Lett.* **87**, 217 (1982).
35. Full local-mode notation is $(v_1,v_2)^{\pm} v_b$, where $v_1$ and $v_2$ specify the number of stretching quanta in O-H bonds 1 and 2, the sign gives the symmetry with respect to interchanging $v_1$ and $v_2$, and $v_b$ gives the number of bending quanta present. Because all of the states studied in this report have $v_b = 0$, this part of the notation is suppressed. Normal mode designations for the $(4,0)^-$, $(5,0)^-$ and $(8,0)^+$ states studied here are (301), (401), and (800) respectively.
36. In the $(8,0)^+$ experiments, the vibrational population was achieved in two sequential steps; one laser pulse promotes ground state molecules to $(4,0)^-$, and a second laser excites the $(4,0)^-$ to $(8,0)^+$ transition, see (*29*).
37. K. K. Lehmann, *J. Chem. Phys.* **95**, 2361 (1991).
38. J. Tennyson, J. R. Henderson, N. G. Fulton, *Comput. Phys. Commun.* **86**, 175 (1995).
39. Most of the required energies are available in J. Tennyson, N. V. Zobov, R. Williamson, O. L. Polyansky, and P. F. Bernath, *J. Phys. Chem. Ref. Data* **30**, 735 (2001). Some of the $(8,0)^+$ term values have been measured in this work.
40. S. V. Shirin, N. F. Zobov, O. L. Polyansky, J. Tennyson, in preparation.
41. Dipole moment matrix elements connecting the experimentally observed eigenstates to all other states are generated without constraints or having to explicitly consider vibrational state mixing. In these calculations, all values of $\mu_{ij}^2/W_{ij} > 0.0001$ Debye$^2$/cm$^{-1}$ were retained. As examples of the complete nature of the calculation, connections between $(4,0)^-0$ and $(1,0)^-7$ and between $(5,0)^-0$ and $(4,0)^-2$ are among the terms included in the *C* coefficients listed in Table 1.
42. O. L. Polyansky *et al.*, in preparation.


43. Supported by the Swiss National Science Foundation, Grant Number 2000-59261.99 and by the European Union Training and Mobility Program, Project SPHERS, Contract Number HPRN-CT-2000-00022. The Swiss contribution to this program was provided by OFES No. 99.0031. University College London work was supported by the National Environmental Research Council (U.K.), Engineering and Physical Sciences Research Council (U.K.), the Russian Fund for Fundamental Studies, and the Royal Society. Finally, the authors would like to thank K. Lehmann for his suggestion to use quantum beats for measuring Stark splittings.

8 May 2002; accepted 2 July 2002